

# BDX on-beam background assess and MC validation

M. Battaglieri, A. Celentano, R. De Vita, L. Marsicano  
*Istituto Nazionale di Fisica Nucleare, Sezione di Genova, 16146 Genova, Italy*

M. Bondi, M. De Napoli, N. Randazzo  
*Istituto Nazionale di Fisica Nucleare, Sezione di Catania, Catania, Italy*

G. Kharashvili, E.S. Smith  
*Jefferson Lab, Newport News, VA 23606, USA*

E. Izaguirre  
*Perimeter Institute for Theoretical Physics, Waterloo, Ontario, Canada, N2L 2Y5*

G. Krnjaic  
*Center for Particle Astrophysics, Fermi National Accelerator Laboratory, Batavia, IL 60510*

D. Snowden-Ifft  
*Occidental College, Los Angeles, California 90041, USA*

M. Carpinelli, V. Sipala  
*Università di Sassari e Istituto Nazionale di Fisica Nucleare, 07100 Sassari, Italy*

*and The BDX Collaboration*

## Abstract

In response to the issue raised by JLAB-PAC44 about the experiment proposal *PR-16-001 Dark matter search in a Beam-Dump eXperiment (BDX) at Jefferson Lab* [?] we propose to measure the prompt radiation produced by the interaction of the high intensity 11 GeV electron beam with the Hall-A beam dump. The muon and neutron flux will be sampled at different height (with-respect-to the beam line), positions and angles downstream of the beam dump to map out the radiation field in the location of the future hall hosting the BDX experiment. In order to realistically assess the beam-on background experienced by the BDX detector, a specimen of the CsI(Tl) crystal from the BDX electromagnetic calorimeter, will be exposed to the radiation as part of a plastic scintillator hodoscope built specifically for this measurement (BDX-Hodo). Although it will not be possible to directly compare results of this tests with the experimental set up proposed in PR-16-001 that will make use of a different and optimised shielding, the measurement will be extremely useful to validate the MonteCarlo simulation tools (GEANT4 and FLUKA) used to design the new underground facility and optimize the BDX detector.

This report is organised as follow: results of the simulation of the radiation field produced by the interaction of the beam with the dump are reported in Sec. ??; the experimental set-up and the detector is described in Sec. ??; the expected results of the measurement are reported in Sec. ?. Details about cost estimate to run the test, work -and time-planes are reported in the Appendix.

## Contents

DRAFT

# 1 MC simulations

## 1.1 The Hall-A high-power beam-dump

The Hall A and C use identical high-power absorbing (up to 1 MW) beam-dumps to stop the 11 GeV beam, remnant of beam/target interaction. The dump is made by a set of about 80 aluminum disks, each approximately 40 cm in diameter of increasing thickness (from 1 to 2 cm), for a total length of approximately 200 cm, followed by a solid Al cylinder 50cm in diameter and approximately 100 cm long. They are both cooled by circulating water. The full drawing of the beam-dump is shown in Fig. ???. To increase the radiation shielding, the thickness of the concrete tunnel surrounding the Al dump is about 4-5 m thick.

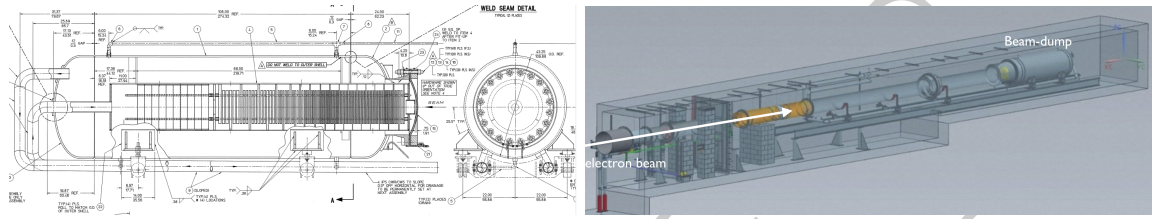


Figure 1: Hall-A beam dump and beam dump enclosure.

## 1.2 The beam-dump model in FLUKA

The beam-dump geometry and materials have been implemented in FLUKA-2011.2c.5 by the Jefferson Lab Radiation Control Department. Detailed are reported in Ref. [?]. The input card used to run the program includes all physics process and a tuned set of bias to speed up the running time not affecting the results integrity. The  $\mu$ , n, and  $\gamma$  fluence (differential in angle and energy)

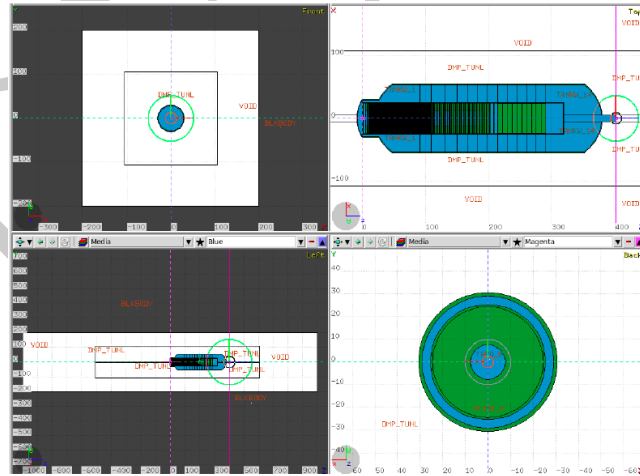


Figure 2: Hall-A beam-dump implementation in FLUKA.

per EOT were calculated at XXX cm downstream of the beam window, through a circular area of

$105\text{ cm}^2$ . Figure ?? shows the FLUKA graphic representation and the location of the flux detector. An extension to also include the proper geometry and material composition downstream of the beam-dump has also been implemented. Figure ?? shows the geometry of the concrete bunker surrounding the beam-dump and the soil as implemented in FLUKA.



Figure 3: The geometry/composition of the concrete bunker surrounding the beam-dump and the soil as implemented in FLUKA.

### 1.3 The beam-dump model in GEANT4 (GEMC)

The beam-dump model, as well as the geometry and composition of surrounding proximity, has also been implemented in GEANT4 using the GEMC tool [?]. This is a refined version with-respect-to the one used in PR-16-001 [?] that better matches the beam-dump geometry implemented in FLUKA. For a better description of muon transportation, the `G4GammaConversionToMuons` has been added to the standard physics list used in simulations of PR-16-001(`FTFP_BERT_HP + STD + HP`). Particles fluence has been sampled by mean of a flux detector has been positioned in the same location as in the FLUKA model. Figure /ref shows the beam dump and vicinity implemented in GEMC.

### 1.4 Radiation of beam/dump interaction

A comparison of muon fluence downstream of the beam-dump (see above for details about the location) obtained by FLUKA and GEMC are reported in Fig. ???. Considering that low energy muons are absorbed by the bunker-head shielding, to keep the GEMC running time reasonable, only particles (all) with energy grater than 100 MeV (`ENERGY_CUT=100*MeV`) has been tracked and sampled. A total of  $4 \times 10^9$  ( $9 \times 10^6$ ) EOT have been simulated with GEMC (FLUKA). The comparison of the two simulations shows a perfect agreement in the full energy range where data were generated. In



Figure 4: The geometry/composition of the beam-dump, the surrounding concrete bunker and the soil as implemented in GEMC.

spite of a factor of  $\times 100$  less statistics, FLUKA shows, as expected, smaller error bars. This reflects the optimised sizes used by the simulation to generate high statistics for low probability processes keeping the total statistics limited. To penetrate the concrete shielding and the soil, minimum energy of  $E_\mu > 4$  GeV is required. With this energy cut, the integrated number of muon per EOT results in  $4.8 \pm 0.1 \times 10^{-7}$  ( $5.5 \pm 0.2 \times 10^{-7}$ ) for GEMC and FLUKA respectively. Figure ?? show the correlation between the muon energy and the azimuthal angle (with-respect-to the beam-line): the regions that are populated by both simulations, show again, the same behaviour.

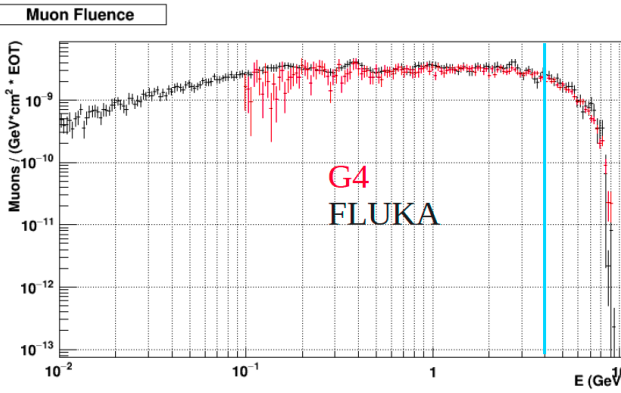


Figure 5: Muon fluence downstream of the beam-dump obtained by FLUKA (black) and GEMC (red). The GEMC simulations started at  $E_\mu = 100$  MeV.

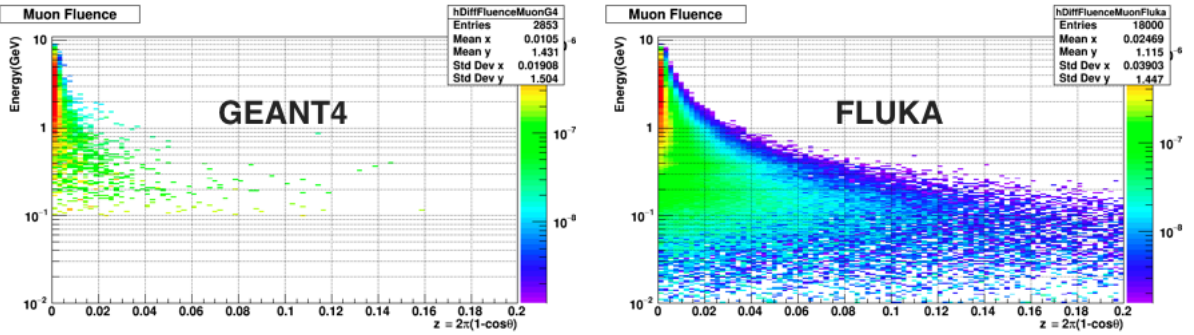


Figure 6: Energy vs. azimuthal angle of muons crossing the flux detector located downstream of the beam-dump obtained by FLUKA and GEMC.

## 1.5 Sampling and particle transport

The good agreement between two independent simulation tools (FLUKA and GEMC) gives us confidence about reliability of the obtained results. Both methods have pros and cons. FLUKA shows a superior speed in running but a complicated implementation and of selected results (e.g. the final output is given via *scores* such as fluence or distribution in specific location need to be pre-defined). GEMC (GEANT4) tracks particles in all volumes providing a straightforward output (particle four-momenta) in the desired flux detector but requires an un-practical running time to collect a reasonable statistics (in particular when an em shower is involved). In the following we describe how we overtook these difficulties.

### 1.5.1 Muons - GEMC

We used GEMC to simulate muons. To make the process more efficient, we defined the following procedure:

- use a low statistic sample of EOT to simulate the interaction of the 11 GeV electrons with the beam-dump;
- sample the muon flux and variables (momentum, azimuthal angle and transverse position) on a flux detector located downstream of the beam-dump;
- use the distributions from previous step as input of a custom event-generator to produce a high statistic muon sample;
- use GEMC to transport muons downstream of the beam dump all the way up the desired location of the BDX-Hodo;
- implement the BDX-Hodo response in GEMC to realistically describe the muon detection.

The position where muons are sampled from the primary beam/dump interaction and generated in the custom-made event generator is shown in Fig. ??.

Figure ?? shows the muon distributions (energy vs azimuthal angle and radial distance from the beam line) downstream of the beam-dump, as obtained by the full GEMC simulation of 11

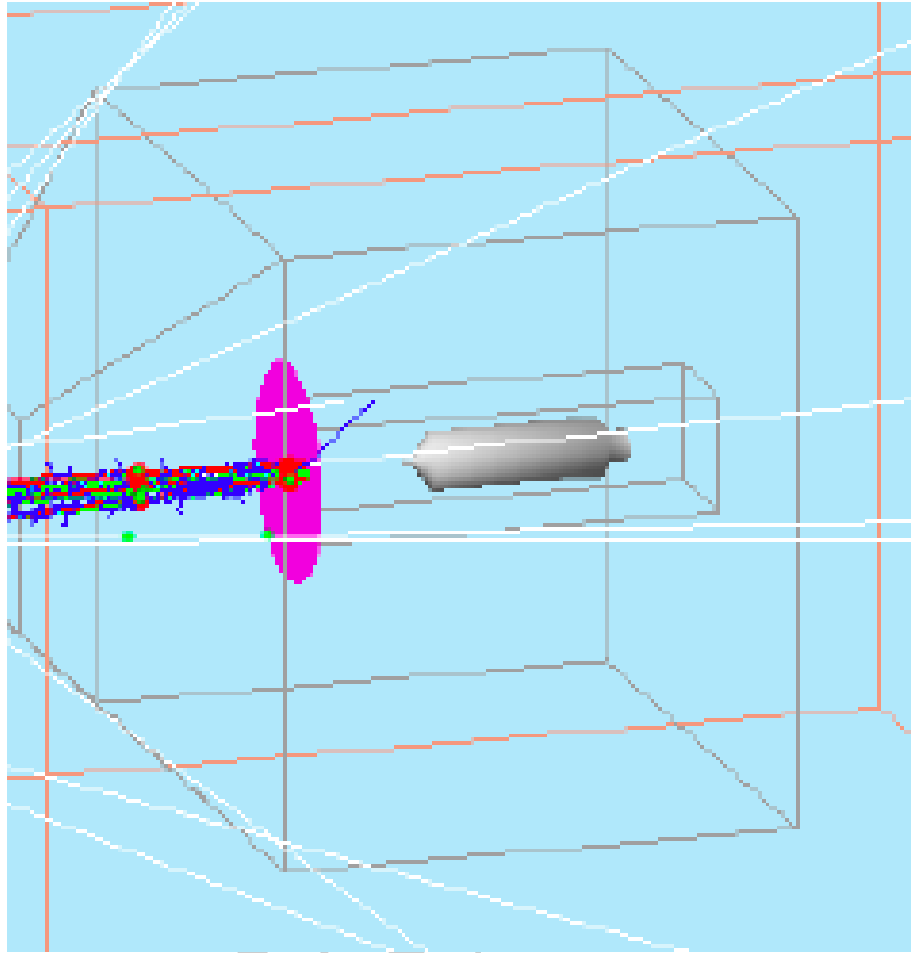


Figure 7: The position of  $\mu$  sampling/generation.

GeV electrons hitting the beam-dump. The left panel of Fig. ?? shows the comparison one of the two distributions as obtained by the GEMC with the result of the custom event generator. As a check, the right panel of the same figure shows the same comparison in the location of interest,  $\sim 20$  m downstream of the beam-dump. The difference in the error bar size indicates the improvement obtained by this procedure with-respect-to the limited statistic from GEMC.

### 1.5.2 Neutrons - FLUKA

Unfortunately the same procedure can not be applied to neutron simulation. Generation and propagation of low energy neutrons (down to thermal energy) prevent the use of a reasonable energy cut-off in GEMC. Moreover, a sizeable contribution to the neutron fluence at the location of interest (in the proximity of the future experimental hall) is given by neutron generated by high energy muons penetrating into the concrete shielding and soil. Given the difficulty in separate the generation (for the primary 11 GeV electron beam interaction and from secondary nuclear processes) from the neutron transport, we decided to only rely on FLUKA.

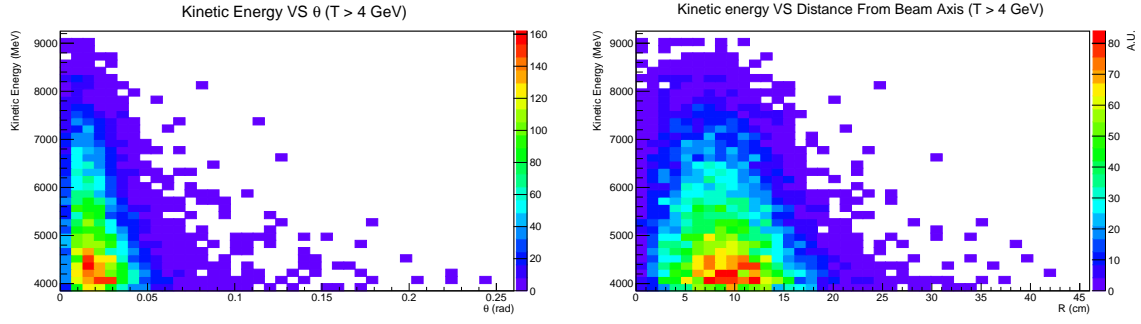


Figure 8: Muon kinetic energy vs. azimuthal angle (left) and distance (right) from the beam-line axes.

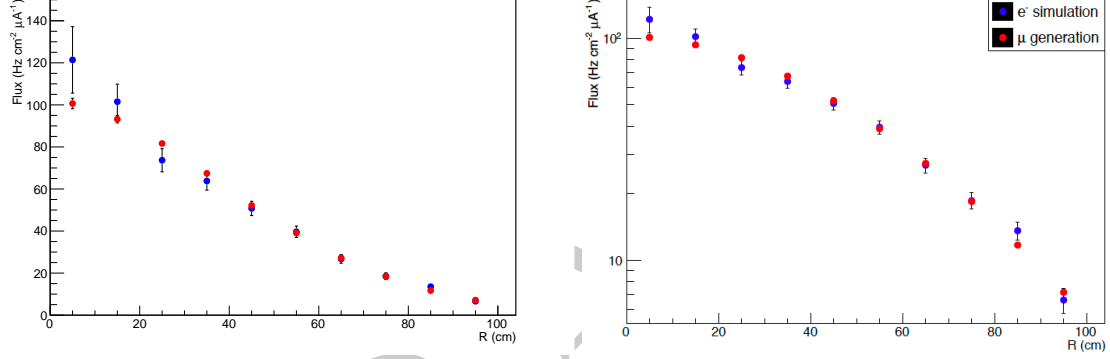


Figure 9: Muon kinetic energy vs. radial distance from the beam-line axes obtained by GEMC (blue) and by the custom event-generator (red) at the sampling/ generation location (left) and in the region of interest (right)  $\sim 20$  m downstream of the beam-dump.

Muon and neutron flux at the location of interest will be discussed in details in the Sec. ?? after presenting in the next Section, the proposed experimental set up and the BDX-Hodo detector.

## 2 Test set-up

### 2.1 Detector location

The area downstream of Hall-A beam-dump is shown in Fig. ?? together with the corresponding location with-respect-to the new underground facility proposed in PR-16-001 [?]. The three positions, indicated with markers **A**, **B** and **C**, correspond to the hall entrance, a middle point and the exit, respectively. The experimental set-up we are proposing assumes to dig a well and insert a pipe in one (or more) of these locations. The BDX-Hodo detector will be lowered in the pipe and muon flux sampled at different height wrt. the beam-line nominal height. The muon flux profiles in Y (vertical direction), measured in different location in Z (distance from the dump) will allow us to compare the absolute and relative MC predictions.

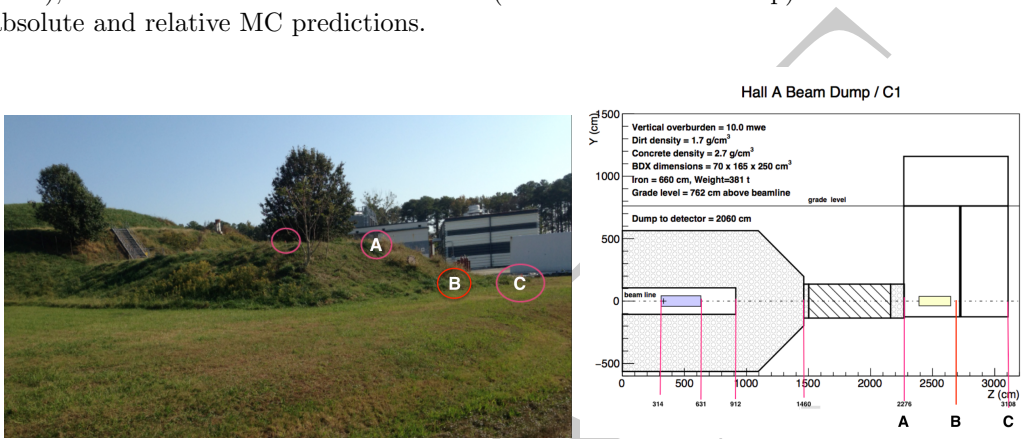


Figure 10: The area downstream of the Hall-A beam-dump and the studied test locations.

### 2.2 The BDX-Hodo detector

The detector used to measure the muon and neutron radiation in the proximity of the new BDX underground facility will make use of a BDX ECal CsI(Tl) crystal sandwiched between a set of segmented plastic scintillators. A CAD representation as well as cuts with sizes are shown in Fig. ???. The front of the crystal will be equipped with two layers of plastic scintillators, each of them composed by a large and a small 1cm-thick scintillators strips. The overlap of the four paddles (each 20 cm long in Y) results in three independent 2.5 cm channels along the X (horizontal) direction. The same concept was applied to the back side of the crystal but with paddles tilted by 90 degrees to define three 2.5 cm independent channels along the Y (vertical) direction. The requirement of a hit in both front and back paddles defines a 3x3 matrix of  $2.5 \times 2.5 \text{ cm}^2$  pixels providing a cm-like XY position resolution. The addition of a larger paddle ( $20 \times 14.4 \text{ cm}^2$ ) on the back provides an enhanced sensitivity in the unlikely case rates will be much lower than what estimated by MC simulations. Four more paddles covering the left/right sides and the top/bottom of the crystal will be used to veto cosmic rays and other radiation not associated to the beam direction. The crystals will be coupled, on the large side, to a  $6 \times 6 \text{ mm}^2$  Hamamatsu S13360-6025 SiPM as described in Sec. 3.2.1 of PR-16-001 [?]. The scintillator paddles will be made with extruded plastic, each read out via a WLS fiber coupled to a  $3 \times 3 \text{ mm}^2$  Hamamatsu S12572-100 SiPM sharing the same technology used in the BDX Inner Veto detector (described in details in Sec. 3.2.2 of PR-16-001). Muons produced by the electron beam will be detected by requiring a 5-fold coincidence (two front paddles + CsI(Tl)

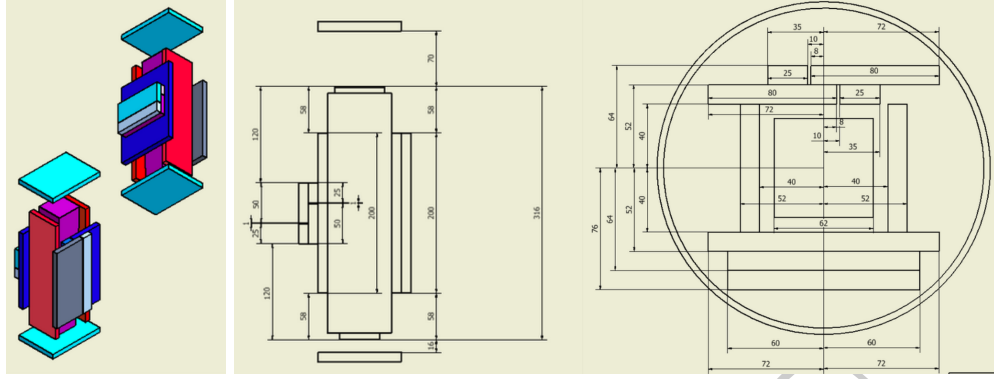


Figure 11: The CAD representation of the BDX-Hodo detector and some drawings with geometry and sizes.

crystal + two back paddles) while neutrons will be detected requiring XXX ... The detector will be contained in a 20-cm diameter stainless-steel cylindrical vessel, covered on top and on the bottom by steel lids. The whole assembly will be water-tight to prevent any water leak inside the vessel. A stainless-steel extension to the top cover will be used to run signal and power cables from the detector to the ground. The extension, made by a 1-inch stainless steel pipe, rigidly attached, will be used also to remotely control the cylinder rotation and provide a good accuracy in the define the angle wrt. the beam direction. The electronics necessary to record the 13 (scintillators) + 1 (crystal) channels require 1 fADC board inserted in a VME crate. The full DAQ system (crate + pc) will be host in a van parked close to the well entrance. The power will be provided by a diesel power generator to minimize the requirements of long extension cords.

### 2.3 GEMC simulation

The detector geometry as well the realistic response of the CsI(Tl) and plastic scintillators have been implemented in GEMC (see Appendix B.2 of PR-16-001 [?] for details about the crystal and plastic scintillator response parametrisation). Figure ?? shows the BDX-Hodo implementation in GEMC.

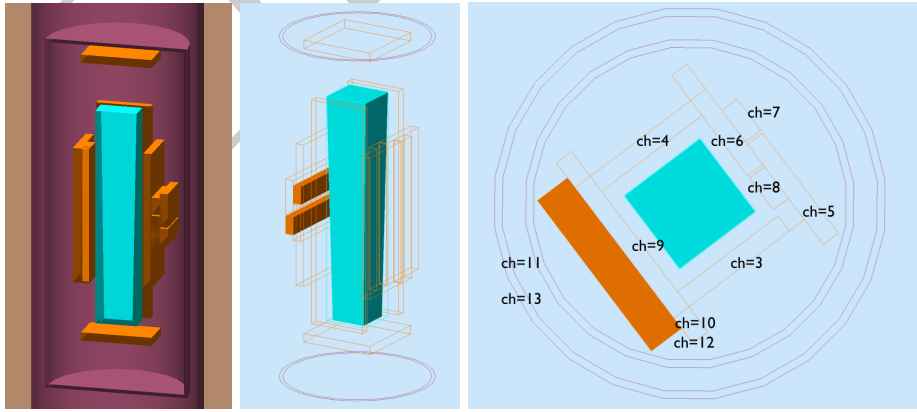


Figure 12: The GEMC implementation of the BDX-Hodo detector.

### **3 Results**

- 3.1 Expected muon rates**
- 3.2 Expected neutron rates**
- 3.3 The proposed set up**

DRAFT

## **4 Appendix**

### **4.1 Cost estimates**

### **4.2 Work-plan, time-plan, ...**

DRAFT